Material Property NMR Imaging of Cross-Linked Polymers Based on Longitudinal Relaxation in the Rotating Frame

P. Barth and S. Hafner*

Fraunhofer-Institut für Biomedizinische Technik, Ensheimer Strasse 48, D-66386 St. Ingbert, Federal Republic of Germany

P. Denner

Pädagogische Hochschule Erfurt/Mühlhausen, Institut für Physik, Nordhäuser Strasse 63, D-99089 Erfurt, Federal Republic of Germany

Received June 6, 1995; Revised Manuscript Received October 3, 1995[⊗]

ABSTRACT: Material property (MAP) NMR imaging is a promising tool for the investigation of materials. It is based on relaxation weighted imaging, which is combined with a theoretical description to relate the measured NMR data, in this investigation represented by $T_{1\rho}$ relaxation values, with the property of the material one is interested in. Following this concept, $T_{1\rho}$ images with different strengths of the spin-lock amplitude have been acquired for a rubber sample consisting of three pieces of natural rubber with different cross-link densities. The data were evaluated using a defect diffusion model and transformed into images of the properties of the polymer network. Images related with the cross-link density and the power law of the $T_{1\rho}$ dispersion, which characterizes the molecular dynamics, have been calculated.

Introduction

Originally developed for clinical investigations, NMR imaging nowadays increasingly is applied for the investigation of materials.[1] Compared with other imaging methods which are used in material science, NMR imaging gives relatively poor resolution. The use of NMR imaging for the investigation of materials, however, is not so much based on high spatial resolution, but rather on its nondestructiveness and on the fact that it allows one to acquire supplementary information on the sample, which is not accessible by other methods.

A technique which was found to be especially useful in this respect is parameter-selective NMR imaging. Parameter-selective NMR imaging is based on the calculation of an image of a suitable NMR parameter, for instance the transverse relaxation time T_2, from a set of different relaxation weighted conventional NMR images. It has been applied so far for the study of cross-link densities, aging processes and the stress distribution in elastomer materials.[1−7] In particular the relaxation times $T_{1\rho}$ (longitudinal relaxation time in the rotating frame) and T_2 (transverse relaxation time) were shown to be sensitive parameters for the discrimination of differently aged regions or of regions with different cross-link densities in rubber samples, respectively.[2−7]

Materials scientists, however, are interested not so much in images of NMR parameters such as relaxation times but in images of properties they use to characterize materials. In previous publications,[3−7] therefore, the first steps toward the imaging of material properties have been undertaken. As a particularly promising approach, the concept of material property (MAP) imaging has been introduced[3] on the example of spin−spin relaxation weighted images, using a single chain model[8−10] for the evaluation of the material properties. Cross-link densities,[3] the correlation times of the chain dynamics, and aging effects[4,5] have been investigated locally and were displayed directly as an image of the corresponding material property. In this work, the concept of MAP imaging will be applied to the other parameter, $T_{1\rho}$, which was found to be sensitive to the structure and dynamics of polymer materials.

Theory

The defect diffusion model has been shown to be useful for the interpretation of $T_{1\rho}$ relaxation in rubber networks[11−15] and, therefore, will be applied in the following for the evaluation of the $T_{1\rho}$ imaging data.

For an uncorrelated homonuclear two-spin system coupled by dipole−dipole interaction, the longitudinal relaxation in the rotating frame is given by[12]

$$\frac{1}{T_{1\rho}} \cong \frac{1}{4} M_{2,\mathrm{mod}} J^{(0)}(2\omega_1) \tag{1}$$

$M_{2,\mathrm{mod}}$ is the fraction of the second moment of the rigid lattice, which is modulated by the molecular motion[12] and $J^{(0)}(2\omega_1)$ is the spectral density function, which is related to the autocorrelation function of the dipolar interaction function $K_0(t)$ by

$$J^{(0)}(2\omega_1) = \int_0^\infty K_0(t) \mathrm{e}^{2i\omega_1 t}\, \mathrm{d}t \tag{2}$$

In the defect diffusion model, the detectable motions of a chain are described as translational diffusion of structural defects, for instance rotational isomers, along parts of the chain. If a defect passes a reference nucleus, which is used as a probe for the molecular motions, the nucleus changes to a perturbed state.

The following assumptions are made for the determination of the correlation function of the molecular motion:

1. The random motions of chain defects are regarded as one-dimensional translational defect diffusion.

2. The molecular motions of the chain defects between chemical and physical cross-links and other topological restrictions are anisotropic, since the restrictions are fixed for the relevant time scale.

3. The chemical cross-links, the physical cross-links, and the topological restrictions are barriers reflecting

* To whom correspondence should be addressed. Present address: Max-Planck-Institut für Polymerforschung, Postfach 3148, D-55021 Mainz.

[⊗] Abstract published in *Advance ACS Abstracts,* January 15, 1996.

0024-9297/96/2229-1655$12.00/0

the diffusing defects. They have an infinite life time compared to the correlation time of motion.

4. A hyperbolic diffusion equation is assumed to account for the limited number of diffusion steps, which are possible between two restrictions in the case of high cross-link density and high defect density.

The assumptions 1−4 lead to a lengthy spectral density function.[12] This function can be simplified for three limiting ranges:

$$J(2\omega_1) = 2\sqrt{2\pi}\frac{1}{\left(\sqrt{\frac{\tau_d}{\tau_b}} - 1\right)}\left(\frac{\tau_b}{2\omega_1}\right)^{1/2}$$

for $\omega_1\tau_b \ll 1$; $\omega_1\tau_d < 1$ (3)

$$J(2\omega_1) = 8\sqrt{\frac{\tau_b}{\tau_d}}\sqrt{1 + \frac{\tau_b}{(\sqrt{\tau_d} - \sqrt{\tau_b})^2}}\frac{1}{2\omega_1}$$

for $\omega_1\tau_b \leq 1 < \omega_1\tau_d$ (4)

$$J(2\omega_1) = \frac{2}{\sqrt{2}}\frac{1}{1 - \sqrt{\frac{\tau_b}{\tau_d}}}\frac{1}{\sqrt{\tau_b}(2\omega_1)^{3/2}}$$

for $\omega_1\tau_b > 1$; $\omega_1\tau_d \gg 1$ (5)

where τ_d is the diffusion time of a diffusing chain defect of the width b over the distance d from barrier to barrier. τ_d is related to the correlation time of the restricted translational diffusion process

$$\tau_c = \frac{1}{K_0(0)}\int_0^\infty |K_0(t)|\, dt \quad (6)$$

by

$$\tau_c \cong \frac{4}{3}\tau_d\left(1 + \frac{2}{\frac{d}{b} - 2}\right) \quad (7)$$

The correlation time τ_c contains all parameters of the model. An increase in the density of chemical cross-links leads to an increase in the correlation time of the defect motion. τ_b is the mean "holding time" of a distortion by a defect at a reference segment and is given by

$$\tau_b = \left(\frac{b}{d - 2b}\right)^2\tau_d \approx \left(\frac{b}{d}\right)^2\tau_d \quad (8)$$

The latter approximation is valid for $d \gg b$.

As can be shown by bulk measurements of $T_{1\rho}$ in rubber at room temperature, the relevant range for the evaluation of the images is the range corresponding to eq 3. Substituting τ_b/τ_d by $(b/d)^2$ and τ_b by τ_d, eq 3 can be written in the following form:

$$J(2\omega_1) = 2\sqrt{2\pi}\frac{1}{\frac{d}{b}\left(\frac{d}{b} - 1\right)}\left(\frac{\tau_d}{2\omega_1}\right)^{1/2} \quad (9)$$

If certain frequencies in the spectrum of motion are frozen, the observed frequency dependence, however, may change as a function of the cross-link density to

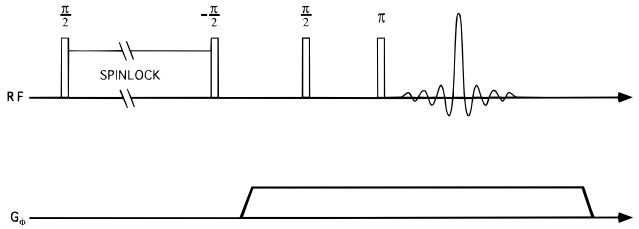

Figure 1. Pulse sequence used for the $T_{1\rho}$ MAP imaging. A spin-lock sequence with flip-back pulse is applied preceding a conventional back-projection spin-echo imaging sequence. The duration of the spin-lock pulse is stepped for the evaluation of the $T_{1\rho}$ values, and the spin-lock amplitude is incremented for the determination of the $T_{1\rho}$ dispersion, which is required for the calculation of the material properties.

ω^α with α between 0 and $^2/_3$. Following the treatment of ref 16, eq 3 is modified to

$$J(2\omega_1) = 2\sqrt{2\pi}\frac{1}{\frac{d}{b}\left(\frac{d}{b} - 1\right)}\frac{t_d^{1-\alpha}}{(2\omega_1)^\alpha} \quad (10)$$

with $0 < \alpha < ^2/_3$.

The final formula for the evaluation of the $T_{1\rho}$ data then is given by

$$\frac{1}{T_{1\rho}(2\omega_1)} = \frac{\pi}{\sqrt{2}}M_{2,\mathrm{mod}}\frac{1}{\frac{d}{b}\left(\frac{d}{b} - 1\right)}\frac{\tau_d^{1-\alpha}}{(2\omega_1)^\alpha} \quad (11)$$

The relevant parameter is d/b, which describes the relation between the diffusion length d and the width of the defect b. For a very small defect concentration along a chain, the diffusion length can be interpreted as the mean length of the inter-cross-link chain and is inversely proportional to the cross-link density. For a given defect width b, the ratio b/d therefore directly reflects the cross-link density of the investigated sample. In general, the parameter d/b is strongly correlated to the distance between physical or chemical cross-links, respectively. The correlation time τ_c, and hence τ_d, can be determined by a temperature dependent bulk measurement from the minimum of $T_{1\rho}(1/T)$,[12] provided that it can be regarded as a constant over the whole sample. For the investigated rubber materials the value for τ_d ($\tau_d \approx 3\tau_c/4$) is 7×10^{-8} s at room temperature. This value is in good agreement with the data from the relaxation map of natural rubber[17] and the well-known William, Landel, Ferry time−temperature equation, respectively. The second moment $M_{2,\mathrm{mod}}$, which is modulated by the motion of structural defects[18,19] (e.g. kinks, Boyer, Schatzki, and Wunderlich crankshaft motion, Boyd−Breitling "flip-flop" motion and gauche translation, Gronsky motion), is regarded to be a constant for the whole sample and is approximately 1.25×10^{10} s^{-2}.

Method

Figure 1 shows the pulse sequence used for the acquisition of the $T_{1\rho}$ images. A conventional spin-echo back-projection imaging sequence is combined with a $T_{1\rho}$ filter sequence. Since the spin-lock pulse becomes slice-selective if it is irradiated under the influence of a gradient,[20] the imaging gradients were switched on after the $T_{1\rho}$ filter. In order to avoid fast gradient switching, which was not possible with the hardware used for the experiment, a flip-back pulse is applied at the end of the $T_{1\rho}$ filter to store the magnetization in the z-direction.

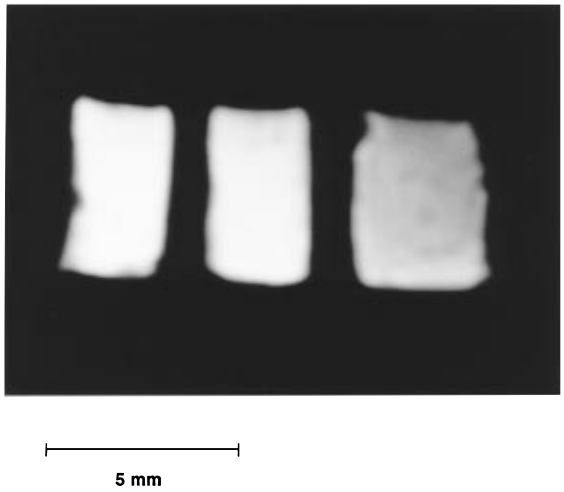

Figure 2. Conventional spin-density image of a sample consisting of three pieces of rubber with different cross-link densities. The values of the cross-link density are (from the left to the right): 3.8×10^{-5}, 6.6×10^{-5}, and 9.8×10^{-5} mol/cm^3. These differences are not represented in the spin-density image.

According to eq 11, the rf-frequency dependence of $T_{1\rho}$ has to be determined for the evaluation of the material parameters. Hence, a series of $T_{1\rho}$ images with different spin-lock amplitudes has to be acquired. The duration of the spin-lock pulse, therefore, is incremented for the acquisition of the $T_{1\rho}$ values, while the lock amplitude is incremented for the determination of the frequency dependence of $T_{1\rho}$.

The evaluation of the acquired data sets is performed in two steps. First, $T_{1\rho}$ images are calculated pixel for pixel from the differently relaxation weighted images. The pixels of the resulting $T_{1\rho}$ images then are used for the determination of the relevant material parameters by a fit of eq 11 using an iterative Levenberg−Marquardt algorithm. The fit procedure is stable as long as reasonable starting values are chosen. For each of the pixels, therefore, an automatic procedure for the estimation of these values is performed prior to the fitting procedure. With a reliability of 90% d/b is determined within 4% and α within 20%. The resulting parameter sets of d/b and α are displayed in the form of the corresponding images.

Experiments and Results

The experiments have been performed on a Varian Unity-400 NMR spectrometer equipped for micro-imaging. A Varian broad-band probe, which was improved by a homemade 5 mm coil insert, was used. The 90° pulse length with this arrangement was 1.5 μs. The spin-lock time was incremented between 100 μs and 3 ms in 24 steps. The amplitudes of the spin-lock pulses were 22.3, 46.3, 67.6, 102.4, and 151.5 kHz, respectively. A gradient of 35 G/cm was stepped by 128 angle increments for the projection-reconstruction procedure. The pixel resolution of the 256 × 256 pixel image was 70 μm × 70 μm. No slice selection was applied to the sample, so that the resolution in the third direction was the thickness of the sample (1.3 mm). The acquired data were evaluated using our homemade image processing software,[21] which is particularly suitable for the analyzation of relaxation weighted NMR images.

The sample was composed of three pieces of filler-free natural rubber with different cross-link densities. The rubber pieces were prepared of standardized Malaysian rubber, which was mixed with an increasing amount of cross-linking agent (0.8, 1.6, and 2.4 phr). The resulting values of the cross-link density have been determined by an alternative NMR method based on transverse relaxation to be 3.8×10^{-5}, 6.6×10^{-5}, and 9.8×10^{-5} mol/cm^3, respectively.[3,9,10]

Figure 2 shows a conventional spin-density image of the first sample. The different cross-link densities of the three rubber pieces cannot be distinguished in this image. The situation changes as soon as the $T_{1\rho}$ weighted sequence is applied and images with cross-link-density induced contrast can be achieved as a basis for the evaluation in terms of material properties.

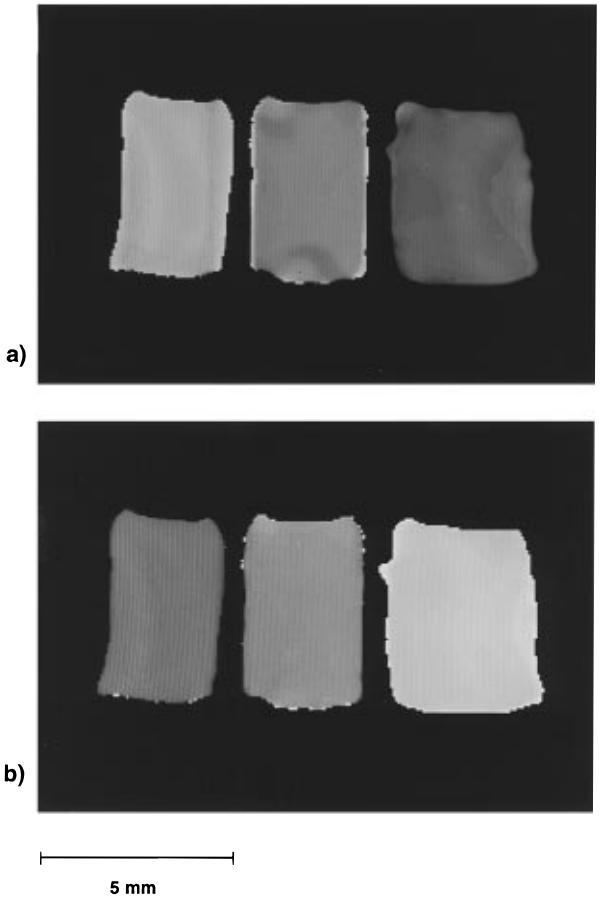

Figure 3. (a) MAP image of the sample of Figure 2. Displayed is the parameter d/b, describing the defect diffusion length in relation to the defect length. The three rubber pieces are easily discriminated by this parameter, since the d/b values are correlated to the cross-link densities. (b) MAP image of the parameter α describing the influence of cross-linking on the spectral density of the molecular motions of the chain defects. For the investigated sample, the values of the parameter α are found to be between 0.1 and 0.25.

Figure 3a shows the resulting d/b image of the sample, where τ_d was regarded to be a constant over the whole sample. In this image, the three pieces of rubber are easily discriminated by their different d/b values. As is expected, the d/b values are decreasing with increasing cross-link density.

Figure 3b shows the corresponding image of the parameter α, which is sensitive to changes in the spectrum of molecular motions. As is evident from the image, also this parameter yields contrast between the different rubber pieces, indicating small changes in the molecular dynamics.

The distribution of the calculated material parameters within the whole sample can be displayed in the form of a histogram analysis. As an example, the d/b distribution is shown in Figure 4a. The three maxima correspond to the center values of d/b for the single rubber pieces. They are well separated from each other, which is an indication of the reliability and accuracy of the fit procedure. From the width of each of the corresponding peaks, the distribution of the d/b values within the rubber pieces can be estimated. Hence, the histogram analysis offers an estimation of the cross-link density inhomogeneity of the single rubber pieces.

For comparison of the model-dependent d/b values with the model-free $T_{1\rho}$ relaxation time, Figure 4b depicts the histogram analysis of a $T_{1\rho}$ image, which was acquired at a field strength of 67.6 kHz. Comparison of both histograms shows that the original $T_{1\rho}$ contrast is preserved by the interpretation in terms

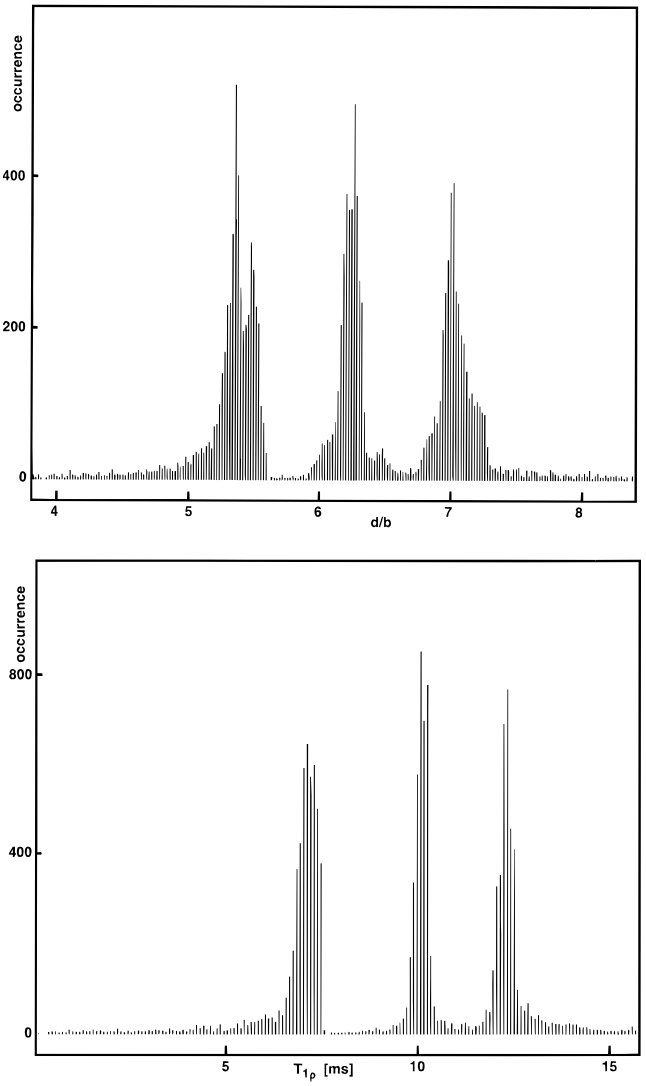

Figure 4. (a) Histogram analysis of the *d*/*b* distribution over the whole sample. The three maxima corresponding to the center values of the three rubber pieces are well separated from each other. The width of the peaks gives an estimation of the cross-link density inhomogeneity of each of the three rubber pieces. (b) Histogram analysis of a $T_{1\rho}$ image of the sample for comparison with Figure 4a. In contrast to the *d*/*b* values, the $T_{1\rho}$ values are not model dependent. By comparison of both histograms it is evident that the contrast information of the original $T_{1\rho}$ values is preserved by the interpretation in term of the defect diffusion model, which confirms the reliability of the corresponding numerical procedures.

of the defect diffusion model and also ensures the reliability of the applied numerical procedures.

Discussion

Material property imaging with $T_{1\rho}$ as the NMR parameter was shown to be a useful tool for the investigation of the properties of rubber materials. The calculation of the MAP images is based on the defect diffusion model, which not only reveals material properties such as the parameter *d*/*b* which is related to the cross-link density but also gives valuable information on the type of motion involved.

Three pieces of rubber with different cross-link densities were used as a test sample for the demonstration of the performance of the method. The different cross-link densities could clearly be distinguished in the material property images and the corresponding histograms. The contrast with respect to the cross-link density for $T_{1\rho}$ MAP imaging was considerably better than the contrast provided by a corresponding MAP image calculated from transverse relaxation.[3,4]

Unlike the single chain model, which was used for the interpretation of transverse relaxation, the defect diffusion model applied here provides the ratio *d*/*b* as a material parameter rather than the cross-link density. In order to evaluate the cross-link density distribution, one has to assume that the defect width b remains the same over the investigated sample. This is certainly a reasonable assumption as long as the spatial variation of the relevant parameters which influence the defect width, such as for instance the cross-link density or the temperature, is relatively small. On the other hand, if the cross-link density distribution is known, for example from transverse MAP imaging, $T_{1\rho}$ MAP imaging in principle enables one to investigate changes in the width of the defects.

Compared with MAP imaging based on transverse relaxation, a certain drawback of $T_{1\rho}$ MAP imaging is that two successive fitting procedures are necessary for the evaluation of the material parameters, one for the calculation of the $T_{1\rho}$ values and the other for the calculation of the material properties from the $T_{1\rho}$ values. Errors in the fitting procedures accumulate and form a big challenge for quantitative evaluations. As a first step toward reliable quantification, detailed investigations of statistical errors are currently in progress. Besides the statistical errors discussed above, a systematic error is introduced by the approximation in eq 8, which is valid for low cross-link density only. For high cross-link density, full eq 8 has to be used and *b* and *d* have to be treated as separate fit parameters.

The acquisition of $T_{1\rho}$ MAP images is very time-consuming, since both the duration and the length of the spin-lock pulses must be varied for the evaluation of the material parameters. However, compared with MAP imaging based on transverse relaxation, $T_{1\rho}$ MAP imaging is less sensitive with respect to artifacts. For instance, the truncation artifact discussed in ref 3 can be easily avoided. But, more important, both techniques are not so much in competition with each other, but give supplementary information on the investigated material. While transverse relaxation MAP imaging directly reveals the cross-link density, $T_{1\rho}$ MAP imaging in addition yields information on the extension of defects and the type of motion involved.

Conventional parameter-selective imaging, certainly, also provides contrast for the investigated sample. However, contrary to relaxation weighted imaging, MAP imaging directly reveals the material and dynamical parameters involved. Material scientists, therefore, are not depending on vague ideas about the relationship between NMR parameters and material properties, but get direct access to the parameters they are interested in. In this context, it should be emphasized that MAP imaging, as it was described above, is not based on a simple transformation of NMR parameters to material parameters in the sense of a simple scaling procedure, but on the interpretation of the measured NMR data using a physical model.

Acknowledgment. Financial support by the Deutsche Forschungsgemeinschaft and the Ministère de l'Education Nationale de Luxembourg is gratefully acknowledged.

References and Notes

(1) Blümich, B., Kuhn, W., Eds. *Magnetic Resonance Microscopy*; VCH: Weinheim, 1992.

(2) Kuhn, W.; Theis, I.; Köller, E. *Mater. Res. Soc. Symp. Proc.* **1991**, *217*, 33.
(3) Kuhn, W.; Barth, P.; Hafner, S.; Simon, G.; Schneider, H. *Macromolecules*, **1994**, *27*, 5773.
(4) Hafner, S.; Barth, P. *Magn. Reson. Imag.* **1995**, *13*, 739.
(5) Fülber, C.; Blümich, B.; Unseld, K.; Hermann, V. *Kautsch. Gummi Kunstst.* **1995**, *48*, 254.
(6) Smith, S. R.; Koenig, J. L. *Macromolecules* **1991**, *24*, 3496.
(7) Blümler, P.; Blümich, B. *Acta Polym.* **1993**, *44*, 125.
(8) Gotlib, Y. Y.; Lifschitz, M. J.; Shevelev, V. A.; Lishanski, J. S.; Balanina, J. V. *Vysokomol. Soedin. A* **1976**, XXVIII, *10*, 2299.
(9) Simon, G.; Götschman, B.; Matzen, D.; Schneider, H. *Polym. Bull.* **1989**, *21*, 475.
(10) Simon, G.; Baumann, K.; Gronski, W. *Macromolecules* **1992**, *25*, 3624.
(11) Kimmich, R.; Voigt, G. *Z. Naturforsch.* **1978**, *33a*, 1294.
(12) Denner, P.; Götz, H. *Wiss. Z. Paedagog. Hochsch. Erfurt* **1987**, 61.
(13) Denner, P.; Götz, H. *Wiss. Z. Paedagog. Hochsch. Erfurt*, **1984**, *2*, 99.
(14) Denner, P.; Götz, H. *Wiss. Z. Paedagog. Hochsch. Erfurt* **1986**, *2*, 131.
(15) Kuhn, W.; Denner, P. *Macromolecules*, in press.
(16) Lenk, R. *Brownian Motion and Spin-Relaxation*; Elsevier Scientific Publishing Co.: Amsterdam, 1977.
(17) Lindberg, J. J.; Törmälä, P. *Europhys. Conf. Macromol. Phys.* **1981**, *51*, 129.
(18) Wunderlich, B. *J. Chem. Phys.* **1962**, *37*, 2469.
(19) Gronski, W. *Macromol. Chem.* **1977**, *178*, 2949.
(20) Hafner, S.; Rommel, E.; Kimmich, R. *J. Magn. Reson.* **1990**, *88*, 449.
(21) Barth, P.; Brill, R.; Staemmler, M.; Kuhn, W. In *Magnetic Resonance Microscopy*; Kuhn, W.; Blümich, B., Eds.; VCH Weinheim: Weinheim, 1992; p 85.

MA950787R